Precise Positioning for Healthcare Robotics with Retroreflective Tags in 5G Small Cell Networks

Alireza Famili*, Tolga O. Atalay†, Angelos Stavrou*†‡
*WayWave Inc, Arlington, Virginia, USA
†A2 Labs LLC, Arlington, Virginia, USA
‡Department of Electrical & Computer Engineering, Virginia Tech, Virginia, USA
afamili@waywave.com, tatalay@a2labs.com, angelos@vt.edu

***Abstract*—The deployment of service robots in healthcare facilities—ranging from autonomous medication delivery carts to patient-assisting mobile platforms—is expanding across diverse applications. To carry out these tasks effectively, there is a pressing need for precise indoor positioning. While global navigation satellite system (GNSS) reliably supports outdoor localization, their performance degrades significantly in indoor settings. In this work, we introduce *REFINE: Retroreflective FR2 Indoor Navigation Engine*, a high-accuracy localization scheme for indoor robotics leveraging low-cost 5G small cells operating in high-frequency bands in conjunction with retroreflective tags. Our approach effectively mitigates synchronization challenges and multipath interference by exploiting the 5G positioning reference signal (PRS) and the unique Van Atta array properties of the tags. We conduct a comprehensive simulation campaign using realistic system parameters and channel models for 5G-enabled deployments in hospital environments. Our results demonstrate that REFINE achieves superior accuracy compared to conventional 5G-based localization techniques, consistently delivering positioning errors below 5 cm in the majority of tested scenarios.**

***Index Terms*—healthcare robotics, indoor localization, 5G small cells, retroreflective tags, passive RTT**

I. Introduction

The integration of robotic platforms in healthcare facilities has gained significant traction in recent years [1]. Automated delivery robots such as the Aethon TUG [2], for instance, are increasingly being adopted to transport medications, laboratory specimens, and meals within hospitals. These mobile systems reduce manual labor, minimize human errors, and improve operational efficiency. In addition, other service-oriented robots assist with disinfection, patient monitoring, and even remote telepresence for medical consultations [3]. As healthcare environments continue to embrace such technologies, the need for robust and reliable solutions that ensure autonomous navigation and task execution becomes more pronounced [4].

A key prerequisite for autonomous robotic operations is accurate localization [5]. Conventional methods based on vision sensors [6] can be expensive, data-intensive, and vulnerable in low-visibility settings or dynamically changing indoor conditions. Alternatively, radio-frequency (RF) fingerprinting techniques using received signal strength (RSS) [7] or channel state information (CSI) [8] often depend on site-specific models and extensive offline training, making them susceptible to real-time environmental variations [9]. In contrast, ranging-based localization strategies inherently offer higher accuracy by measuring time of flight (ToF) or phase of arrival (PoA). While global navigation satellite system (GNSS) networks work well outdoors [10], [11], they suffer considerable performance degradation in enclosed spaces due to signal blockage and multipath [12], [13]. Even in scenarios where GNSS services are available, their maximum accuracy may not suffice for applications demanding higher localization precision.

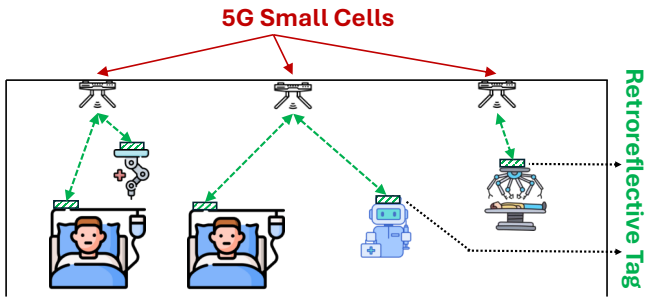

Fig. 1: Overview of REFINE framework in a healthcare environment, with 5G small cells mounted on the ceiling and mobile units equipped with retroreflective tags for precise positioning.

In this paper, we introduce ***REFINE: Retroreflective FR2 Indoor Navigation Engine***, a novel indoor localization framework designed specifically for healthcare robotics as illustrated in Figure 1. Unlike conventional schemes that rely on large outdoor 5G base stations [14], our solution employs cost-effective and compact 5G small cells mounted throughout hospital floors. These small cells transmit positioning reference signal (PRS) sequences in high-frequency bands, such as frequency range 2 (FR2), to achieve high-resolution ranging.

Recent studies on reconfigurable intelligent surface (RIS) technology have explored its deployment in the environment to shape RF propagation [15]. However, one study [16] took an unconventional approach by mounting RIS on a drone, using it merely as an RF mirror—an overly complex and impractical setup for this purpose. Instead, REFINE leverages ultra-low-power retroreflective tags based on Van Atta arrays. These tags act as RF mirrors, reflecting incoming signals back along the exact path they arrived from. Beyond lowering system complexity, this approach inherently addresses synchronization challenges and mitigates multipath interference. To showcase its versatility, we evaluate REFINE across three popular frequencies in the FR2 band (e.g., 26 GHz, 28 GHz,

ISBN 978-3-903176-72-0 © 2025 IFIP

and 39 GHz), which are commonly allocated in different global regions, ensuring broad applicability. The primary contributions of our work are as follows:

- We introduce REFINE, a high-accuracy localization system tailored for healthcare robotics operating in complex indoor environments.
- REFINE leverages cost-effective and easily deployable indoor 5G small cells operating in high-frequency FR2 band with up to 800 MHz bandwidth, enabling dedicated PRS transmissions for enhanced positioning accuracy.
- REFINE employs ultra-low-power retroreflective tags based on Van Atta arrays, which act as RF mirrors to reflect PRS signals back to the 5G small cells.
- By returning the signal via the same path, REFINE alleviates stringent synchronization requirements between the robot and the small cells, mitigates adverse multipath effects, and significantly reduces power consumption and computational demands on the robot side.
- We enhance the MATLAB 5G Toolbox with additional models and optimizations and conduct a comprehensive simulation campaign using realistic hospital environment parameters. Our results show that REFINE outperforms state-of-the-art 5G localization techniques, achieving an overall positioning error below 5 cm in most scenarios.

The remainder of this paper is structured as follows. In Section II, we provide some background and discuss related work relevant to our study. Next, we detail the REFINE architecture in Section III, followed by a theoretical analysis of its ranging error bound in Section IV. Section V presents our simulation setup and performance evaluation. Finally, Section VI concludes the paper with a summary of our findings and potential avenues for future research.

II. Related Work & Background

Our proposed approach lies at the intersection of three key areas: robotics in healthcare, localization techniques, and retroreflective technology. Below, we review the major contributions and challenges in each domain.

Robotics in Healthcare: Robotic platforms have become an integral component of modern healthcare settings, facilitating a wide range of tasks [17]. Some of the most notable implementations include automated pharmacy robots that dispense medications with high accuracy, disinfection robots employing ultraviolet-C (UV-C) light to sanitize patient rooms, and assistive robots that deliver meals or transport laboratory specimens. For instance, the Aethon TUG [2] system has been extensively deployed in hospitals to carry linens, medications, and meals between different wards, helping to reduce the manual workload on healthcare professionals. Similarly, telepresence robots enable remote consultations, significantly improving patient access to specialized care. These diverse applications underscore the transformative potential of robotic automation in enhancing both clinical efficiency and patient outcomes. However, reliable autonomous navigation remains a crucial requirement for widespread adoption, as any mislocalization may compromise patient safety and reduce workflow efficiency.

Indoor Localization Techniques: A variety of positioning methods have been developed for indoor scenarios, each with its own strengths and limitations [18]–[20]. Vision-based techniques often utilize simultaneous localization and mapping (SLAM) [21] or advanced image processing algorithms [22] to build and update an environmental map. While highly accurate under stable lighting and minimal occlusion conditions, vision systems can become unreliable when faced with poor illumination, cluttered environments, or unexpected obstacles [23].

Fingerprinting methods, which rely on radio-frequency features such as RSS [7] or CSI [8], offer an alternative by matching real-time measurements to a pre-recorded database. Although these solutions can be simple to deploy using existing wireless infrastructure, they demand extensive offline data collection and calibration. Furthermore, any significant change in the indoor layout (e.g., moving furniture or walls) can substantially degrade positioning performance [9].

Ranging-based strategies have emerged as a more robust alternative, leveraging measurements like time of arrival (ToA) [24], time difference of arrival (TDoA) [25], or angle of arrival (AoA) [26]. In ToA systems, the distance is inferred from the one-way travel time of a signal, necessitating strict time synchronization between the transmitter (user) and the receiver (anchor) [27]. This synchronization can be challenging in practical indoor environments due to fluctuating clock drifts and multipath propagation. TDoA, on the other hand, circumvents the synchronization issue by measuring the difference in arrival times across multiple anchors, thereby eliminating clock offset bias and relaxing synchronization requirements [28]. AoA relies on antenna arrays to estimate the incoming signal's angle but typically requires elaborate hardware and high computational overhead for direction finding. In each of these ranging-based methods, the final step of position estimation can be performed through trilateration when distance information is available or angulation when angular information is used.

Retroreflective Technology: Retroreflective tags originated in the field of optics [29], where they have long been used on traffic signs and safety gear to reflect light back to its source [30]. In the RF domain, Van Atta arrays are a prominent example of retroreflective technology [31]. These arrays are designed so that the signal received on each element is re-radiated back along the incident path, effectively acting as an "RF mirror." Traditional implementations of RF retroreflectors were limited to continuous wave signals, where the primary application was to enhance radar cross-section or simplify radio frequency identification (RFID)-like sensing. Recent advancements, however, have demonstrated the feasibility of using retroreflective tags with modulated signals [32], such as orthogonal frequency-division multiplexing (OFDM)-modulated cellular network signals.

To the best of our knowledge, we are the first to propose a localization system that employs ranging-based techniques in high-frequency 5G bands while using retroreflective tags to simplify synchronization and mitigate multipath. By leveraging 5G small cells and the full potential of wide-band PRS transmissions alongside the retroreflective tag on the user side (i.e., the robot), our approach achieves both high-resolution ranging and a dramatically reduced processing burden on the user side.

III. REFINE Architecture

This section presents the architecture of REFINE, highlighting how our proposed 5G-based framework addresses indoor positioning challenges without incurring high power usage or heavy synchronization demands. Unlike conventional approaches that rely on active transmitters on the user equipment (UE) or complex multi-anchor synchronization, REFINE leverages mmWave 5G small cells and retroreflective tags to simplify operations and significantly reduce power consumption. We begin by outlining the relevant 5G system model and reviewing two key methods in the 3rd generation partnership project (3GPP) standards, observed time difference of arrival (OTDoA) and round trip time (RTT). Next, we revisit RIS to show how prior attempts to modify the propagation environment led to unnecessary complexity. Finally, we introduce the core contribution of REFINE: the utilization of retroreflective tags as low-power substitutes for active user transmitters, alongside the conclusion of REFINE's localization scheme.

A. REFINE Small Cell Deployment

In this work, we capitalize on 5G New Radio (NR) technology to enable high-precision indoor positioning. As illustrated in Figure 2, traditional macrocell towers often provide insufficient coverage inside large healthcare facilities, primarily due to attenuated signals and obstructed lines of sight. Instead, we deploy *small cells*, which are compact base stations connected to the same 5G core network infrastructure. By installing multiple small cells on the ceilings of hospital corridors and rooms, we gain finer-grained control over coverage, mitigate outdoor path-loss issues, and ensure a line of sight (LoS) for each cell within its intended area.

5G NR frequency ranges are broadly split into FR1 (sub-6 GHz) and FR2 (millimeter-wave). While FR1 accommodates wide-area coverage, its limited bandwidth restricts ranging resolution. Conversely, FR2—operating above 24 GHz—offers substantially larger bandwidth (hundreds of MHz), translating to higher time resolution and improved positioning accuracy. In our design, we utilize FR2 channels centered at three representative bands: 26 GHz, 28 GHz, and 39 GHz. Each of these frequencies is widely adopted in different global regions, for instance, 28 GHz in parts of the US, 26 GHz in Europe, and 39 GHz across multiple markets, ensuring the broad applicability of our approach.

Let N be the number of indoor small cells deployed throughout the facility, each with a known coordinate $\mathbf{p}_i = (x_i, y_i, z_i)$, $i = 1, 2, \ldots, N$. During operation, each small cell periodically transmits 5G PRS on its assigned FR2 band, leveraging the generous bandwidth to achieve fine-grained distance measurements. A mobile robot travels on the hospital floor with a retroreflective tag mounted on it. The key objective is to estimate the robot's position $\mathbf{r} = (x, y, z)$ in real time. In many healthcare settings, movement is predominantly on the ground, so height may be treated as known; however, the formulation extends naturally to three-dimensional (3D) deployments if vertical motion or multi-floor environments must be considered.

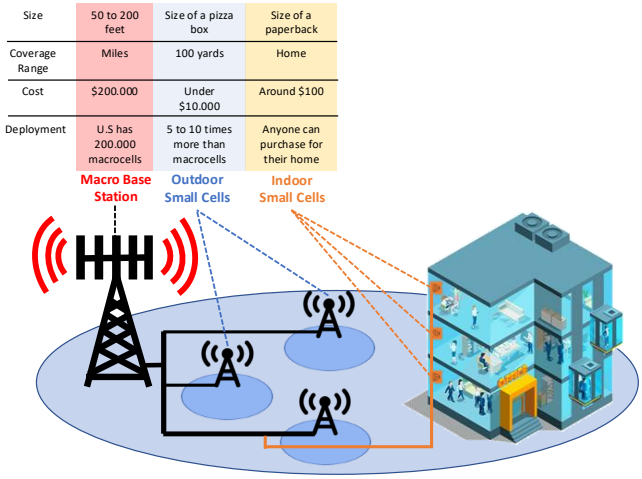

Fig. 2: Various deployments in 5G heterogeneous networks.

B. Time-Based Localization

In 5G networks, the two primary time-based techniques standardized by 3GPP for positioning are OTDoA and RTT. Both methods seek to improve localization accuracy by measuring signal travel times, but each tackles the device-to-network synchronization challenge in distinct ways. In the following subsections, we briefly outline their core principles and drawbacks. Later, we explain how REFINE builds on these standard protocols to further enhance positioning accuracy while reducing power consumption and complexity.

1) OTDoA: This method exploits the differences in signal arrival times from multiple anchors to eliminate the unknown UE clock bias. Suppose the i-th small cell transmits a PRS signal $s_i(t)$ at time $t = 0$. The UE receives this signal at time:

$$t_i = \tau_i + \tau_0, \tag{1}$$

where $\tau_i = \frac{\|\mathbf{r}-\mathbf{p}_i\|}{c}$ is the one-way propagation delay (with c the speed of light), and τ_0 encapsulates the UE's clock offset relative to the network. Here, $\|\cdot\|$ denotes the Euclidean norm, i.e., $\|\mathbf{r} - \mathbf{p}_i\| = \sqrt{(x - x_i)^2 + (y - y_i)^2 + (z - z_i)^2}$, which represents the Euclidean distance between the UE position $\mathbf{r} = (x, y, z)$ and the anchor position $\mathbf{p}_i = (x_i, y_i, z_i)$. Instead of computing absolute ToA, OTDoA calculates the differences:

$$\Delta t_{ij} = t_i - t_j = (\tau_i + \tau_0) - (\tau_j + \tau_0) = \tau_i - \tau_j. \tag{2}$$

Hence, the unknown τ_0 cancels out, leaving only the differences in geometric propagation delays:

$$\Delta t_{ij} = \frac{\|\mathbf{r} - \mathbf{p}_i\| - \|\mathbf{r} - \mathbf{p}_j\|}{c}. \tag{3}$$

Each Δt_{ij} translates into a hyperbolic constraint in the spatial domain. With measurements from at least four non-collinear small cells, these hyperbolas intersect at the UE's position in three-dimensional space.

2) RTT: An alternative approach is round-trip time localization, where the same anchor transmits a reference signal and measures the time until it is received back. Denote $t_{RTT,i}$ as the measured round-trip time between the i-th small cell

and the UE. If the signal makes a forward and backward pass over distance $\|\mathbf{r} - \mathbf{p}_i\|$, then:

$$t_{RTT,i} = 2\,\frac{\|\mathbf{r} - \mathbf{p}_i\|}{c} \;+\; \delta_i, \tag{4}$$

where δ_i is any residual processing delay at the anchor or the UE. Since both transmission and reception occur at the small cell, the system can effectively calibrate out δ_i or treat it as a fixed offset. Thus, the one-way distance is:

$$d_i = \|\mathbf{r} - \mathbf{p}_i\| = \frac{c}{2}\big(t_{RTT,i} - \delta_i\big). \tag{5}$$

According to several studies (e.g., [16]), RTT-based ranging demonstrates a Cramér-Rao lower bound (CRLB) roughly half that of OTDoA under comparable conditions, which means they have better positioning accuracy. However, conventional RTT requires the UE to actively transmit the return signal making it power-demanding and increasing the computational process.

C. REFINE Ranging Scheme

RIS technologies have emerged as a promising tool in next-generation wireless systems to shape the radio propagation environment. An RIS is typically a two-dimensional (2D) metasurface composed of numerous sub-wavelength elements, each capable of imposing a controllable phase shift to incoming waves. In standard deployments, an RIS is affixed to walls or ceilings, aiding coverage by reflecting beams in desired directions. In [16], Famili et al. proposed an unconventional method by placing the RIS on an aerial drone hovering above the target area.

While their approach validates that RIS-based reflectors can enhance localization by relaxing synchronization requirements, it also introduces complexities. Although the RIS can redirect incoming waves toward any chosen angle, using them solely as a mirror that reflects a signal back to its source is unnecessarily complex and costly. Implementing RIS entails added hardware, complex control of reflection coefficients, and ongoing calibration to set desired angles, which is overkill if the goal is simply to send the signal back along the same path. Consequently, we propose REFINE as a low-power, low-complexity alternative that eliminates these overheads by leveraging inherently retroreflective hardware.

To circumvent the power-hungry nature of actively transmitting UEs (as in RTT) or the heightened cost and complexity of RIS-based approaches, REFINE leverages ultra-low-power retroreflective tags built on the Van Atta array principle, as shown in [31]. In a Van Atta configuration, each antenna element has a paired element so that incoming signals are re-radiated back along precisely the same trajectory from which they arrived. This setup is shown in Figure 3, where a robot is mounted with a retroreflective tag so that any incoming signal is sent back on the incoming angle. Concretely, if a plane wave from angle θ induces a current I_n on the n-th array element, the array is wired such that the re-radiated wave leaves at angle θ in the reverse direction, retaining the incident signal's phase relationships. This "focused mirror" action ensures that reflected energy naturally flows back toward its source, removing the need for high-power active transmissions at the user side.

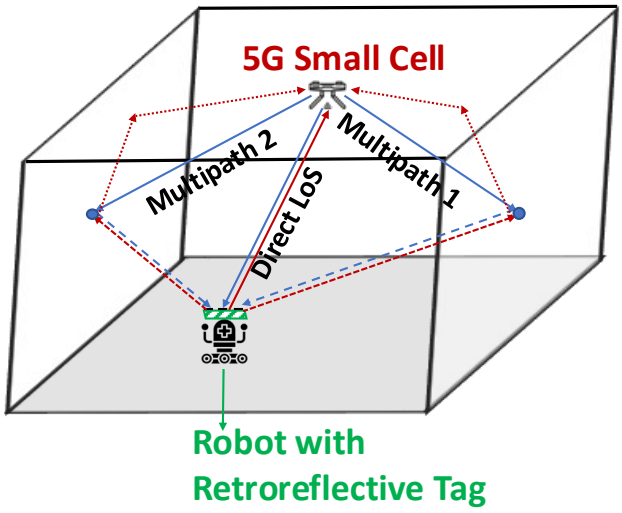

Fig. 3: Retroreflective tag mounted on a robot for categorizing the multipath components and the line of sight (LoS) path.

Signal Model for Retroreflection: Consider a small cell located at $\mathbf{p}_i$ transmitting a PRS signal:

$$x_i(t) \;=\; \sqrt{P_i}\, s(t)\, e^{j2\pi f_b t}, \tag{6}$$

where P_i is transmit power and f_b is the FR2 carrier frequency. An incoming wave at the retroreflective tag excites each antenna element n with:

$$r_n(t) \;=\; \alpha_{n,i}\, x_i\big(t - \tau_{n,i}\big), \tag{7}$$

where $\alpha_{n,i}$ captures path loss and element gain, and $\tau_{n,i}$ is the propagation delay to element n. Van Atta wiring ensures these waves re-radiate coherently back to $\mathbf{p}_i$, yielding:

$$y_i(t) \;\approx\; \beta_i\, x_i\big(t - 2\tau_i\big) = \sqrt{P_i}\, s(t - 2\tau_i)\, e^{j2\pi f_b (t - 2\tau_i)}, \tag{8}$$

where $\tau_i = \frac{\|\mathbf{r} - \mathbf{p}_i\|}{c}$ is the one-way delay, and β_i includes the total round-trip path loss and array gain. Notably, the robot's tag remains passive; the anchor alone measures the round-trip time and computes $d_i = \|\mathbf{r} - \mathbf{p}_i\|$.

Synchronization and Multipath Reduction: Since the small cell both transmits and receives, any clock offset at the user side is irrelevant, reducing the typical synchronization headache in ToA-based positioning. The small cell simply time-stamps $x_i(t)$ and correlates it with $y_i(t)$ upon reflection. Moreover, as shown in Figure 3, multipath signals from environmental reflectors, such as walls, objects in the hospital, clutter, and other obstructions, typically return to their source rather than to the 5G small cell. For instance, if a multipath component arises from the reflection of the primary 5G PRS signal off a wall, the retroreflective tag acts as a mirror, directing the reflected signal back toward the wall instead of the small cell. Consequently, multipath components from environmental reflectors rarely return along the exact path needed to combine coherently. Thus, Van Atta retroreflection inherently suppresses interference from unintended surfaces. The result is a low-complexity, low-power, and multipath-resilient alternative to sophisticated RIS-based solutions, forming the cornerstone of REFINE's passive-RTT localization strategy.

D. REFINE Trilateration

As mentioned earlier, we have N small cells located at known coordinates on the ceiling $\mathbf{p}_i = (x_i,\ y_i,\ z_i)$, for $i = 1, \ldots, N$, and the robot's unknown location is denoted by $\mathbf{r} = (x,\ y,\ z)$. Now, after accurately obtaining the ranging information—thanks to the synchronization-free, multipath-robust ranging scheme in REFINE—we have the distance d_i between the robot and the i-th small cell and can write:

$$\|\mathbf{r} - \mathbf{p}_i\|^2 \ = \ d_i^2, \qquad i = 1, \ldots, N. \tag{9}$$

Expanding Equation (9) yields:

$$(x - x_i)^2 + (y - y_i)^2 + (z - z_i)^2 = d_i^2. \tag{10}$$

Defining a reference anchor (e.g., the N-th small cell) and comparing each i-th with N leads to a set of linear equations in (x, y, z). For $i = 1, 2, \ldots, (N-1)$, we can write:

$$\begin{aligned}\left(d_i^2 - d_N^2\right) - \left(x_i^2 - x_N^2 + y_i^2 - y_N^2 + z_i^2 - z_N^2\right) = \\ -2\Big[(x_i - x_N)\,x + (y_i - y_N)\,y + (z_i - z_N)\,z\Big].\end{aligned} \tag{11}$$

Collecting these into a matrix form $\mathbf{A}\,\mathbf{x} = \mathbf{b}$:

$$\mathbf{A} = \begin{bmatrix} A_{1,1} & A_{1,2} & A_{1,3} \\ A_{2,1} & A_{2,2} & A_{2,3} \\ \vdots & \vdots & \vdots \\ A_{N-1,1} & A_{N-1,2} & A_{N-1,3} \end{bmatrix},\ \mathbf{x} = \begin{bmatrix} x \\ y \\ z \end{bmatrix},\ \mathbf{b} = \begin{bmatrix} b_1 \\ b_2 \\ \vdots \\ b_{N-1} \end{bmatrix},$$

where $\mathbf{x} = \mathbf{r}^{\mathsf{T}} = (x, y, z)^{\mathsf{T}}$, and the elements of $\mathbf{A}$ and $\mathbf{b}$ are as follows:

$$\begin{gathered}A_{i,1} = -\,2\,(x_i - x_N),\ A_{i,2} = -2\,(y_i - y_N),\ A_{i,3} = -2\,(z_i - z_N), \\ b_i \ = \ (d_i^2 - d_N^2) - (x_i^2 - x_N^2 + y_i^2 - y_N^2 + z_i^2 - z_N^2).\end{gathered}$$

If the robot z coordinate is known; in other words, we need to perform location estimation in 2D plane, $N \geq 3$ anchors suffice. Otherwise, $N \geq 4$ is required for a full 3D space localization. A pseudo-inverse solution or least-squares approach gives:

$$\widehat{\mathbf{x}} \ = \ \left(\mathbf{A}^{\mathsf{T}}\mathbf{A}\right)^{-1}\mathbf{A}^{\mathsf{T}}\,\mathbf{b}. \tag{12}$$

In practice, measurement noise implies a least-squares objective is often more robust:

$$\min_{x,y,z} \ \sum_{i=1}^{N}\Big(\|\mathbf{r} - \mathbf{p}_i\| \ - \ d_i\Big)^2, \tag{13}$$

which can be solved via iterative algorithms (e.g., Gauss-Newton) when outliers or non-line-of-sight (NLoS) paths are significant. Regardless, this linear or iterative framework conveniently incorporates the REFINE distances d_i from each small cell to the retroreflective tag, yielding a direct and computationally efficient method for real-time localization.

IV. REFINE Ranging Error Bounds

In this section, we derive the CRLB to characterize the achievable ranging accuracy of REFINE. As in classical estimation theory, the CRLB provides a minimum-variance threshold for any unbiased estimator, equivalently expressed via the Fisher information matrix (FIM). Let θ be an unknown parameter to be estimated from observations x with density $f(x;\theta)$. Then the FIM is as follows and the variance of $\hat{\theta}$ is bounded by the inverse of the FIM:

$$I(\theta) = \mathbb{E}\left[\left(\frac{\partial \ln f(x\,|\,\theta)}{\partial\theta}\right)\left(\frac{\partial \ln f(x\,|\,\theta)}{\partial\theta}\right)^{T}\right],$$

$$\operatorname{var}\big(\hat{\theta}\big) \ \geq \ \frac{1}{I(\theta)}.$$

In a positioning scenario, we focus on the positioning error bound (PEB), defined as the square root of the CRLB on the user's (x, y, z) location. Denoting the unknown coordinate vector by $\boldsymbol{\zeta} = [x \ \ y \ \ z]^{\mathsf{T}}$, we can write:

$$\mathrm{PEB} \ = \ \sqrt{\mathrm{tr}\Big(I^{-1}(\boldsymbol{\zeta})\Big)},$$

where $I(\boldsymbol{\zeta})$ is the FIM for those coordinates and $\mathrm{tr}(\cdot)$ denotes the matrix trace. In ranging-based localization, the PEB is commonly viewed as the product of two factors: the per-link ranging error σ_r and a geometric dilution of precision (GDOP) factor that depends on anchor layout [33]:

$$\mathrm{PEB} \ = \ \sigma(r) \ = \ \sigma_r \cdot \mathrm{GDOP}.$$

In this work, we do not address the GDOP arising from the relative anchor–user layout. Instead, our primary objective is to diminish the latter factor, the per-link ranging error σ_r. As discussed earlier, we propose a passive RTT approach that leverages retroreflective tags on the user with high-frequency 5G small cells installed on the ceiling.

To start, consider the single-link CRLB for distance. Let d be the unknown anchor-to-user distance, $\hat{d}$ its estimate, and $\hat{\tau}$ the estimated one-way ToA. We have

$$\mathrm{CRLB}\big(\hat{d}\big) \ = \ c^2 \cdot \mathrm{CRLB}\big(\hat{\tau}\big),$$

where c is the speed of light. Thus, we first examine $\mathrm{CRLB}(\hat{\tau})$ under typical 5G PRS. In 3GPP Rel. 16 and beyond, PRS is often an OFDM-modulated signal spanning subcarrier spacing Δf. Let the OFDM-modulated PRS signal be as follows:

$$s_i(t) = \frac{1}{\sqrt{N}} \sum_{k=-\frac{N}{2}}^{\frac{N}{2}-1} S_i[k]\ e^{\,j\,2\pi\,k\,\Delta f\,t},$$

where N is the total number of subcarriers, $\Delta f = 1/(N\,T_s)$ is the subcarrier spacing (effective bandwidth per subcarrier), the parameter T_s represents the OFDM symbol duration (without cyclic prefix), and $S_i[k]$ are the symbols. After a channel-induced delay τ plus noise, the receiver samples the incoming signal at discrete time instances $t = nT$, where T is the sampling interval, resulting in a discrete-time received signal:

$$y_i[n] \ = \ s_{R,i}[n] \ + \ n_i[n], \quad n_i[n] \sim \mathcal{CN}(0, \sigma_n^2),$$

where $\mathcal{CN}(0, \sigma_n^2)$ represents complex Gaussian noise with zero mean and variance σ_n^2, and

$$s_{R,i}[n] = \ s_i\big(nT - \tau\big) = \frac{1}{\sqrt{N}} \sum_{k=-\frac{N}{2}}^{\frac{N}{2}-1} S_i[k]\, e^{\,j\,2\pi\,k\,\Delta f\,(nT-\tau)}.$$

If the probability distribution function (PDF) of $\mathbf{y}$ given τ is represented as $p(\mathbf{y} \mid \tau)$, then the variance of the time-delay estimate is bounded by the CRLB, given by:

$$\mathrm{var}\big(\hat{\tau}\big) \;\geq\; \frac{1}{E\Big[\big(\frac{\partial}{\partial \tau} \ln p(\mathbf{y} \mid \tau)\big)^2\Big]}.$$

Under high signal-to-noise ratio (SNR) and uncorrelated subcarriers, we can write it as follows:

$$\mathrm{var}\big(\hat{\tau}\big) \;\geq\; \frac{1}{8\pi^2\,(\Delta f)^2\,\mathcal{K}},$$

where $\mathcal{K} = \frac{1}{\sigma_n^2} \sum_{i=0}^{N_{\mathrm{symbol}}-1} \sum_{k=-\frac{N}{2}}^{\frac{N}{2}-1} k^2\, S_i[k]^2$, and N_{symbol} is the number of OFDM symbols.

Mapping $\tau \to d = c\tau$ scales the variance by c^2, resulting in the single-link distance bound under perfect synchronization between the user and anchor as follows:

$$\mathrm{CRLB}\big(\hat{d}\big) = \frac{c^2}{8\pi^2\,(\Delta f)^2\,\mathcal{K}},$$

$$\sigma_r \;\geq\; \sqrt{\mathrm{CRLB}\big(\hat{d}\big)} = \frac{c}{2\sqrt{2}\,\pi\,\Delta f}\,\sqrt{\frac{1}{\mathcal{K}}}.$$

As described earlier, 5G commonly adopts one of two techniques for managing user clock offsets in time-based positioning: OTDoA and RTT. In OTDoA, the user subtracts the arrival time at one anchor from that at another, eliminating the common synchronization bias but doubling the variance of ranging error. If the baseline single-link ranging variance is σ_r^2 and assuming perfect synchronization among positioning anchors, then OTDoA's variance becomes $2\,\sigma_r^2$. By contrast, RTT centralizes timing at the anchor, which halves the variance, i.e., $\sigma_{r,\mathrm{RTT}}^2$ is about $1/2$ times σ_r^2 [34].

Our proposed REFINE system follows the distance-measurement principle of RTT without requiring an active uplink transmitter at the user side. Consequently, σ_{REFINE} matches $\sigma_{r,\mathrm{RTT}}$, without the requirement of perfect synchronization among anchors, which is required in OTDoA systems. Specifically, to derive the ranging error bound for our retroreflective-based design, we replace $s_i(nT - \tau)$ with $s_i(nT - 2\tau)$, since the flight time doubles when the wave is reflected back to the same anchor. Repeating the partial-derivative steps for τ reveals that:

$$\sigma_{\mathrm{REFINE}} \;=\; \tfrac{1}{\sqrt{2}}\,\sigma_r \;\geq\; \sqrt{\mathrm{CRLB}\big(\hat{d}_{\mathrm{REFINE}}\big)} = \frac{c}{4\,\pi\,\Delta f}\,\sqrt{\frac{1}{\mathcal{K}}}.$$

Thus, under the same bandwidth Δf and SNR, and without requiring stringent synchronization—either between the user and anchor or between anchors (as in OTDoA)—the REFINE design halves the per-link distance ranging error compared to OTDoA. Finally, from $\mathrm{PEB} = \sigma_r \times \mathrm{GDOP}$, this halving of σ_r carries over directly to the final positioning bound, leading to improved localization accuracy.

V. Performance Evaluation

In this section, we assess the performance of REFINE in a realistic hospital-oriented indoor environment. First, we describe the simulation setup in Section V-A. Then, in Section V-B, we provide the overall evaluation results.

A. Simulation Setup

We implement our simulation campaign in MATLAB on a MacBook Pro computer equipped with 64 GB RAM and an Apple M3 Max processor. The scenario mimics a typical hospital floor plan, featuring all the typical clutter and objects in a healthcare environment, with positioning nodes (5G small cells) located on the ceiling to maximize LoS coverage. In most experiments, we model an indoor space with size of $20\,\mathrm{m} \times 20\,\mathrm{m} \times 3\,\mathrm{m}$, although the framework can handle different dimensions for broader assessments.

To maintain realism, we employ the 5G Toolbox in MATLAB to generate downlink PRS and configure the channel. System parameters (e.g., subcarrier spacing, OFDM symbol configuration, PRS frame structure) adhere to 3GPP guidelines. We also set the path-loss and fading characteristics to a cluttered-yet-line-of-sight indoor environment, approximating hospital corridors and open wards. The exact profile—InH configuration, which is designed for indoor hotspot or similar configurations—ensures that simulations reflect plausible multipath effects while still allowing a dominant direct path from anchors on the ceiling.

Each small cell transmits in the FR2 band, where broader allocations facilitate fine time resolution. Specifically, we evaluate three representative frequencies:

- *26 GHz*, widely deployed across parts of Asia and Europe,
- *28 GHz*, a popular choice in North America,
- *39 GHz*, another common mmWave band with large contiguous blocks.

These allow us to showcase how higher frequencies, coupled with wider bandwidth, can yield improved ranging accuracy in REFINE, especially when compared to lower-frequency sub-6 GHz systems.

To capture the effect of signal reflection in our passive retroreflective tags, we simulate the two-hop propagation (anchor →tag →anchor) and include small-fading variations. With ceiling-mounted anchors ensuring predominant LoS, we achieve better coverage to measure for each anchor–tag pair.

B. Overall Results

This part presents the evaluation outcomes for our proposed REFINE scheme. We begin by plotting the localization error's cumulative distribution functions (CDFs) in Figure 4. As discussed previously, REFINE operates at high frequencies in the FR2 range in order to exploit the large available bandwidth for higher timing resolution. Specifically, we use three representative carriers in FR2, namely 26 GHz, 28 GHz, and 39 GHz, all of which are commonly adopted worldwide for 5G mmWave deployments. Each subplot in Figure 4 compares the performance of REFINE at all of these three frequencies, allowing us to observe how the error distribution shifts with different carrier bands and their respective bandwidths.

To assess errors along different coordinates, we present three separate subplots: one for the absolute error along the x-axis, one for the y-axis, and one for the resulting 2D planar localization error. We assume the healthcare robot remains on the floor at a known height, thus we did not provide the z-axis estimation. Nonetheless, our framework supports

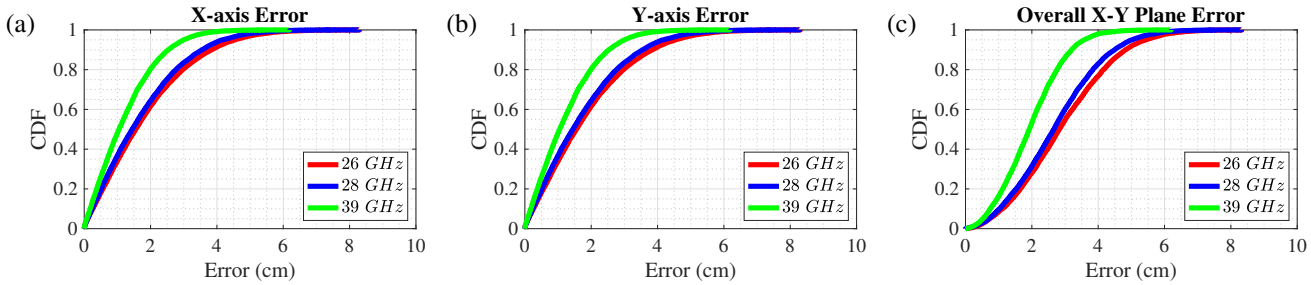

Fig. 4: CDF plots of localization error for (a) the x-axis, (b) the y-axis, and (c) the overall 2D plane. Each plot compares the results from three FR2 carrier frequencies (26 GHz, 28 GHz, and 39 GHz). All errors are reported in centimeters.

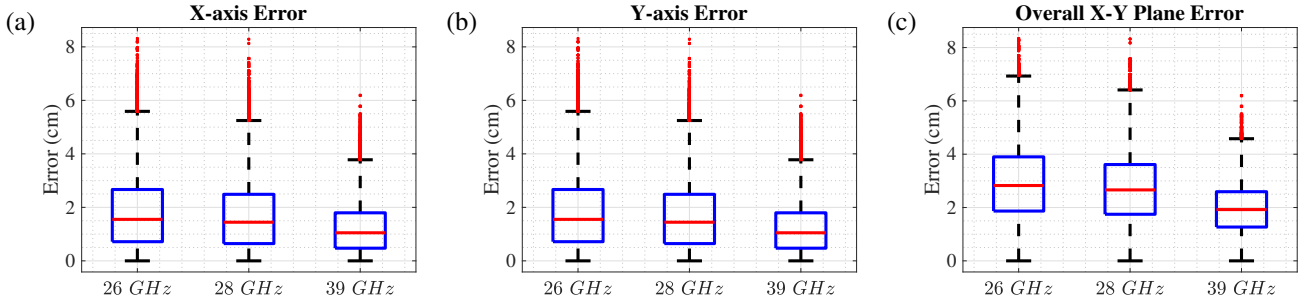

Fig. 5: Boxplots illustrating the localization error for (a) the x-axis, (b) the y-axis, and (c) the overall 2D plane. Each plot compares three FR2 carrier frequencies (26 GHz, 28 GHz, and 39 GHz). Errors are reported in centimeters.

3D positioning if required, as mentioned earlier. At each point in the simulation, we estimate the robot's location using REFINE and compare it against the ground-truth coordinates at that instant; the absolute discrepancy between these two positions defines the error for that point. By aggregating these per-point errors into a CDF, we can readily visualize how frequently REFINE meets specific accuracy thresholds, thereby validating its mmWave-based precision in realistic hospital layouts.

As shown in Figure 4, operating at 26 GHz or 28 GHz (yielding similar performance) keeps 95% of all 2D localization errors under 5 cm. Leveraging the even wider bandwidth at 39 GHz reduces that error threshold to about 2.5 cm. This improvement stands well above the performance of state-of-the-art solutions, enabled by REFINE's innovative approach to mitigate multipath and relax synchronization requirements.

To provide a more detailed view of REFINE's localization accuracy—covering the minimum and maximum error, distribution shape, and notable outliers—we present Figure 5. These boxplots incorporate different carrier frequencies as well as error measurements along each axis and the overall 2D positioning, extending the analysis initiated by Figure 4.

In each boxplot, the lower and upper edges correspond to the 25$^{\text{th}}$ and 75$^{\text{th}}$ percentiles, respectively, capturing the middle 50%, interquartile range (IQR), of the data. The horizontal line within the box denotes the median, illustrating the central tendency. Whiskers extend up to 1.5 times the IQR beyond the box, while any points beyond this range are plotted individually as outliers—highlighting extreme deviations in accuracy. As seen in Figure 5, the median 2D localization error for both 26 GHz and 28 GHz clusters around 3 cm (specifically 2.8 cm at 26 GHz and 2.6 cm at 28 GHz), whereas moving to 39 GHz reduces the median error below 2 cm (down to about 1.9 cm).

Figure 6 compares our proposed REFINE system with the OFDRA system presented in [16], which leverages RIS for localization, and a standard 5G system operating in the sub-6 GHz (FR1) band using RTT for localization. To ensure a fair comparison, we implement both OFDRA and the conventional 5G system in the same environment as REFINE, maintaining identical multipath effects and environmental noise. In other words, all environmental factors—ranging from the size of the indoor healthcare space to the adverse channel effects of noise, multipath, and clutter in the hospital—are kept consistent. Additionally, we maintain uniform conditions for the number of locations where robot position data is collected, the placement of small cells on the ceiling, and all other experimental parameters. This setup guarantees that our comparison accurately reflects the true performance differences between REFINE and other state-of-the-art systems.

As previously discussed, REFINE is designed to operate in the FR2 band and is not restricted to a single carrier frequency. To demonstrate its adaptability, we evaluate REFINE at three widely used and readily available frequencies that do not require additional infrastructure modifications. As shown in Figure 6, REFINE significantly outperforms both OFDRA and the standard 5G RTT system, regardless of the carrier frequency used. Specifically, REFINE achieves an overall 2D localization accuracy of less than 10 cm across all data points. In contrast, the RIS-based localization system proposed in [16] exhibits a localization accuracy of approximately 60 cm, six times worse than REFINE. This discrepancy arises from REFINE's use of a much simpler structure (a Van Atta array for retroreflectivity), which not only reduces error but also makes the system considerably less complex and significantly more power-efficient compared to the computationally intensive RIS-based approach.

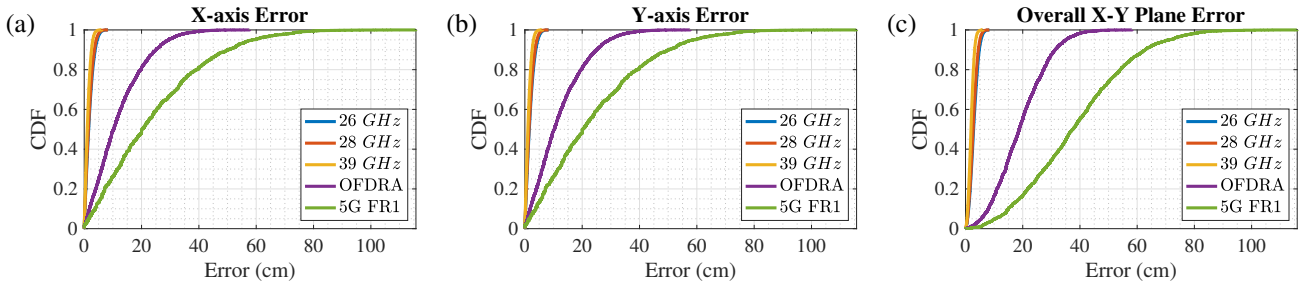

Fig. 6: CDF plots comparing the performance of REFINE, OFDRA [16], and 5G FR1 RTT: (a) along the x-axis, (b) along the y-axis, and (c) in the overall 2D plane. Each plot presents results for three FR2 carrier frequencies (26 GHz, 28 GHz, and 39 GHz) explored in REFINE, compared to OFDRA [16] and a standard 5G system operating in the sub-6 GHz band and using the RTT technique for positioning. All errors are reported in centimeters.

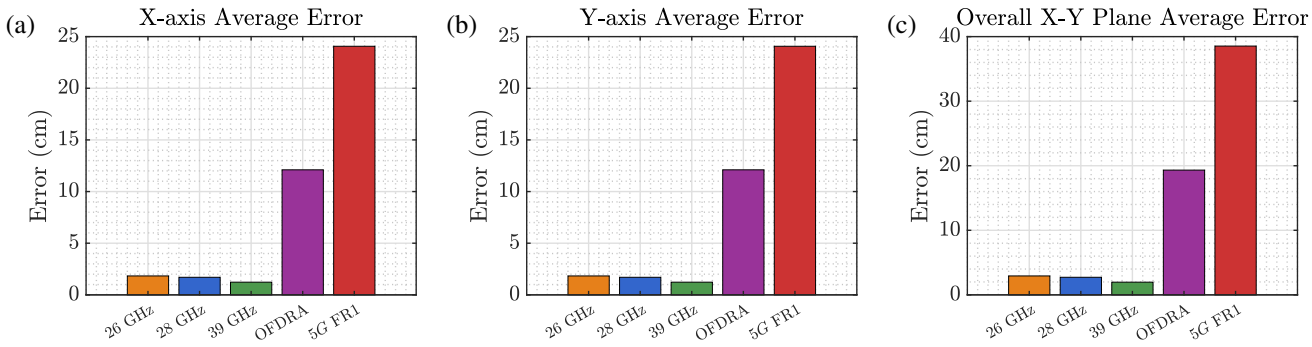

Fig. 7: Bar plots illustrating the average error of REFINE, OFDRA [16], and 5G FR1 RTT: (a) in the x-axis component, (b) in the y-axis component, and (c) in the overall 2D space. Each plot depicts results for three FR2 carrier frequencies (26 GHz, 28 GHz, and 39 GHz) analyzed in REFINE, alongside a comparison with OFDRA [16] and a conventional 5G system operating in the sub-6 GHz band that employs RTT for positioning. All error values are expressed in centimeters.

Furthermore, leveraging the 5G mmWave band provides REFINE with a larger bandwidth, which translates to improved timing resolution and higher ranging accuracy. Finally, when comparing REFINE to the conventional 5G system operating in the sub-6 GHz band with RTT, we observe additional disadvantages in the latter. First, it requires an active user on the robot side, necessitating continuous active transmissions to the small cells. Second, it suffers more significantly from multipath effects compared to our proposed system. As a result, the 2D localization accuracy threshold for the majority of the data in the CDF plot exceeds 120 cm, twelve times worse than what REFINE provides. Therefore, REFINE enhances localization accuracy compared to the state-of-the-art RTT-based positioning scheme in 5G NR by more than an order of magnitude.

Figure 7 presents a comparison of the average ranging error for REFINE, OFDRA [16], and 5G FR1 RTT across different localization dimensions. From left to right, the subfigures represent: (a) the average ranging error for the x-axis estimation, (b) the same metric for the y-axis estimation, and (c) the overall 2D localization error.

To compute the average error, we first estimate the robot's position using the REFINE architecture and then compare it against the ground-truth location at each test point. The average error for the x-axis also known as x-axis mean absolute error (MAE) is calculated as:

$$e_{x,\text{avg}} = \frac{1}{N_T} \sum_{i=1}^{N_T} \sqrt{(x_{\text{REFINE},i} - x_{\text{GT},i})^2},$$

where N_T represents the total number of locations at which the robot's position is estimated, $x_{\text{REFINE},i}$ is the estimated x-coordinate at location i, and $x_{\text{GT},i}$ is the corresponding ground-truth x-coordinate. A similar formula applies to the y-axis:

$$e_{y,\text{avg}} = \frac{1}{N_T} \sum_{i=1}^{N_T} \sqrt{(y_{\text{REFINE},i} - y_{\text{GT},i})^2}.$$

For the overall 2D average error, the formula to calculate $e_{\text{2D, avg}}$ extends as follows:

$$\frac{1}{N_T} \sum_{i=1}^{N_T} \sqrt{(x_{\text{REFINE},i} - x_{\text{GT},i})^2 + (y_{\text{REFINE},i} - y_{\text{GT},i})^2}.$$

Similar to Figure 6, we ensure that all environmental conditions remain identical across all systems to provide a fair comparison. This includes maintaining the same indoor healthcare environment, multipath effects, noise levels, small cell placements, and the number of data collection points.

As observed in Figure 7, REFINE significantly outperforms both OFDRA and the standard 5G FR1 RTT-based positioning systems. The overall 2D average error for REFINE is approximately 3 cm, whereas OFDRA exhibits an average error of 19 cm, and the 5G FR1 RTT-based system results in an average error of 38 cm.

VI. Conclusion and Future Work

Conclusion. In this paper, we introduced REFINE, a high-accuracy localization scheme designed for robotic and

automation use cases in healthcare facilities. By installing 5G small cells on the ceiling and mounting retroreflective tags on indoor robots, REFINE enables the direct mirroring of 5G PRS back to their respective transmitters. This approach addresses two major limitations of conventional 5G positioning. First, it relaxes the need for tight synchronization on the robot side, since the anchor (small cell) alone performs RTT measurements. Second, it substantially mitigates multipath, as only the strongest direct path is re-radiated coherently toward the same anchor, while off-angle reflections return to other unintended sources and thus remain largely inconsequential. Through an extensive simulation campaign using realistic 5G NR parameters and three representative frequencies in the FR2 band, we showed that REFINE achieves significantly lower positioning errors than state-of-the-art baselines.

Future Work. Currently, we are building an extensive 5G testbed in our laboratory, which now operates at sub-6 GHz frequencies using OpenAirInterface [35]. Our next step is to adapt this infrastructure for FR2 mmWave, enabling a deeper real-world evaluation of REFINE beyond simulations.

References

[1] S. Aggarwal, D. Gupta, and S. Saini, "A literature survey on robotics in healthcare," in *2019 4th International Conference on Information Systems and Computer Networks (ISCON)*, 2019, pp. 55–58.

[2] E. U. Aydınocak, "Robotics systems and healthcare logistics," in *Health 4.0 and medical supply chain*. Springer, 2023, pp. 79–96.

[3] D. Sarikaya, J. J. Corso, and K. A. Guru, "Detection and localization of robotic tools in robot-assisted surgery videos using deep neural networks for region proposal and detection," *IEEE Transactions on Medical Imaging*, vol. 36, no. 7, pp. 1542–1549, 2017.

[4] T. D. Than, G. Alici, H. Zhou, and W. Li, "A review of localization systems for robotic endoscopic capsules," *IEEE Transactions on Biomedical Engineering*, vol. 59, no. 9, pp. 2387–2399, 2012.

[5] A. Famili, A. Stavrou, H. Wang, and J.-M. J. Park, "PILOT: high-precision indoor localization for autonomous drones," *IEEE Transactions on Vehicular Technology*, pp. 1–15, 2022.

[6] L. Bai, Y. Yang, M. Chen, C. Feng, C. Guo, W. Saad, and S. Cui, "Computer vision-based localization with visible light communications," *IEEE Transactions on Wireless Communications*, vol. 21, no. 3, pp. 2051–2065, 2022.

[7] N. Singh, S. Choe, and R. Punmiya, "Machine learning based indoor localization using Wi-Fi RSSI fingerprints: An overview," *IEEE Access*, vol. 9, pp. 127 150–127 174, 2021.

[8] Y. Ruan, L. Chen, X. Zhou, G. Guo, and R. Chen, "Hi-Loc: Hybrid indoor localization via enhanced 5G NR CSI," *IEEE Transactions on Instrumentation and Measurement*, vol. 71, pp. 1–15, 2022.

[9] A. Famili, V. Slyusar, Y. H. Lee, and A. Stavrou, "Vehicular teamwork for better positioning," in *2023 IEEE International Conference on Systems, Man, and Cybernetics (SMC)*, 2023, pp. 3507–3513.

[10] S. Cho, J. Lee, G. Park, and W. Chung, "Outdoor mobile robot localization with factor graph and GNSS uncertainty map," in *2024 24th International Conference on Control, Automation and Systems (ICCAS)*, 2024, pp. 1593–1594.

[11] S.-J. Lee, B. Kim, D.-W. Yang, J. Kim, T. Parkinson, J. Billingham, C. Park, J. Yoon, and D.-Y. Lee, "A compact RTK-GNSS device for high-precision localization of outdoor mobile robots," *Journal of Field Robotics*, vol. 41, no. 5, pp. 1349–1365, 2024.

[12] A. Famili, A. Stavrou, H. Wang, and J.-M. Park, "iDROP: Robust localization for indoor navigation of drones with optimized beacon placement," *IEEE Internet of Things Journal*, vol. 10, no. 16, pp. 14 226–14 238, 2023.

[13] J. Song, W. Li, C. Duan, L. Wang, Y. Fan, and X. Zhu, "An optimization-based indoor–outdoor seamless positioning method integrating GNSS RTK, PS, and VIO," *IEEE Transactions on Circuits and Systems II: Express Briefs*, vol. 71, no. 5, pp. 2889–2893, 2024.

[14] A. Famili, M. Foruhandeh, T. Atalay, A. Stavrou, and H. Wang, "GPS spoofing detection by leveraging 5G positioning capabilities," in *2022 IEEE Latin-American Conference on Communications (LATINCOM)*, 2022, pp. 1–6.

[15] Y. Wang, W. Zhang, Y. Chen, C.-X. Wang, and J. Sun, "Novel multiple RIS-assisted communications for 6G networks," *IEEE Communications Letters*, vol. 26, no. 6, pp. 1413–1417, 2022.

[16] A. Famili, T. O. Atalay, A. Stavrou, H. Wang, and J.-M. Park, "OFDRA: Optimal femtocell deployment for accurate indoor positioning of RIS-mounted AVs," *IEEE Journal on Selected Areas in Communications*, vol. 41, no. 12, pp. 3783–3798, 2023.

[17] L. D. Riek, "Healthcare robotics," *Commun. ACM*, vol. 60, no. 11, p. 68–78, Oct. 2017. [Online]. Available: https://doi.org/10.1145/3127874

[18] R. E. Nkrow, B. Silva, D. Boshoff, G. Hancke, M. Gidlund, and A. Abu-Mahfouz, "NLOS identification and mitigation for time-based indoor localization systems: Survey and future research directions," *ACM Comput. Surv.*, vol. 56, no. 12, Oct. 2024. [Online]. Available: https://doi.org/10.1145/3663473

[19] O. Kerdjidj, Y. Himeur, S. S. Sohail, A. Amira, F. Fadli, S. Atalla, W. Mansoor, A. Copiaco, A. Gawanmeh, S. Miniaoui, and D. W. Dawoud, "Uncovering the potential of indoor localization: Role of deep and transfer learning," *IEEE Access*, vol. 12, pp. 73 980–74 010, 2024.

[20] A. Famili, A. Stavrou, H. Wang, and J.-M. Park, "SPIN: sensor placement for indoor navigation of drones," in *IEEE LATINCOM 2022*, nov 2022.

[21] L. Zhuang, X. Zhong, L. Xu, C. Tian, and W. Yu, "Visual SLAM for unmanned aerial vehicles: Localization and perception," *Sensors*, vol. 24, no. 10, 2024. [Online]. Available: https://www.mdpi.com/1424-8220/24/10/2980

[22] A. Morar, A. Moldoveanu, I. Mocanu, F. Moldoveanu, I. E. Radoi, V. Asavei, A. Gradinaru, and A. Butean, "A comprehensive survey of indoor localization methods based on computer vision," *Sensors*, vol. 20, no. 9, p. 2641, 2020.

[23] A. Famili, A. Stavrou, H. Wang, and J.-M. Park, "OPTILOD: Optimal beacon placement for high-accuracy indoor localization of drones," *Sensors*, vol. 24, no. 6, p. 1865, 2024.

[24] H. Wu, L. Liang, X. Mei, and Y. Zhang, "A convex optimization approach for NLOS error mitigation in TOA-based localization," *IEEE Signal Processing Letters*, vol. 29, pp. 677–681, 2022.

[25] A. Famili, G. Himona, Y. Kominis, A. Stavrou, and V. Kovanis, "Isochrons in injection locked photonic oscillators: A new frontier for high-precision localization," *IEEE Journal of Indoor and Seamless Positioning and Navigation*, vol. 2, pp. 304–319, 2024.

[26] E. Y. Menta, N. Malm, R. Jäntti, K. Ruttik, M. Costa, and K. Leppänen, "On the performance of aoa–based localization in 5g ultra–dense networks," *IEEE Access*, vol. 7, pp. 33 870–33 880, 2019.

[27] A. Famili, A. Stavrou, H. Wang, and J.-M. J. Park, "RAIL: robust acoustic indoor localization for drones," in *2022 IEEE 95th Vehicular Technology Conference: (VTC2022-Spring)*, 2022, pp. 1–6.

[28] Y. Sun, K. C. Ho, and Q. Wan, "Solution and analysis of tdoa localization of a near or distant source in closed form," *IEEE Transactions on Signal Processing*, vol. 67, no. 2, pp. 320–335, 2019.

[29] A. Egidi *et al.*, "Review of main optical retroreflectors," *Ist. Naz. Ric. Metrol. Turin Italy Tech. Rep. RT*, vol. 31, p. 2018, 2018.

[30] C. Y. Brown, T. A. Brubaker, A. M. Churchill, G. M. Crosswhite, D. Fried, L. Kirsch, D. A. Zelman, and D. J. Lovell, "Development of an electrophoretic display technology for selectively retroreflective signs and pavement markers," *Journal of Transportation Engineering*, vol. 141, no. 1, p. 04014067, 2015.

[31] E. Soltanaghaei, A. Prabhakara, A. Balanuta, M. Anderson, J. M. Rabaey, S. Kumar, and A. Rowe, "Millimetro: mmWave retroreflective tags for accurate, long range localization," in *Proceedings of the 27th Annual International Conference on Mobile Computing and Networking*, ser. MobiCom '21. New York, NY, USA: Association for Computing Machinery, 2021, p. 69–82. [Online]. Available: https://doi.org/10.1145/3447993.3448627

[32] M. Lotti, N. Decarli, G. Pasolini, and D. Dardari, "Real-time localization based on MIMO backscattering from retro-directive antenna arrays," *IEEE Transactions on Vehicular Technology*, pp. 1–16, 2025.

[33] A. Famili, T. Atalay, A. Stavrou, and H. Wang, "Wi-Six: precise positioning in the Metaverse via optimal Wi-Fi router deployment in 6G networks," in *2023 IEEE International Conference on Metaverse Computing, Networking and Applications (MetaCom)*, 2023, pp. 17–24.

[34] L. Mailaender, "On the geolocation bounds for round-trip time-of-arrival and all non-line-of-sight channels," *EURASIP Journal on Advances in Signal Processing*, vol. 2008, pp. 1–10, 2007.

[35] T. O. Atalay, A. Famili, D. Stojadinovic, and A. Stavrou, "Demystifying 5G Traffic Patterns with an Indoor RAN Measurement Campaign," in *GLOBECOM 2023-2023 IEEE Global Communications Conference*. IEEE, 2023, pp. 1185–1190.